Structure of the crust and upper mantle beneath Bass Strait, southeast Australia, from teleseismic body wave tomography

M. Bello[*1,2], N. Rawlinson[3], D. G. Cornwell[1], E. Crowder[1], M. Salmon[4] & A. M. Reading[5]

[1]School of Geosciences, University of Aberdeen, Aberdeen UK

[2]Department of Physics, Abubakar Tafawa Balewa University, Bauchi, Nigeria

[3]Department of Earth Sciences – Bullard Labs, University of Cambridge, Cambridge, UK

[4]Research School of Earth Sciences, The Australian National University, Canberra, Australia

[5]School of Natural Sciences (Physics), University of Tasmania, Hobart, TAS 7001, Australia

We present new constraints on the lithospheric velocity structure of Bass Strait and the adjoining landmasses of mainland Australia and Tasmania in order to better constrain their geological and tectonic relationship. This is achieved by performing teleseismic tomography using data from fifteen deployments of WOMBAT and BASS transportable arrays, which span southeastern Australia. The starting model for the teleseismic tomography includes crustal velocity structure constrained by surface waves extracted from ambient seismic noise data and a Moho surface and broad-scale variations in 3-D upper mantle velocity structure from the Australian seismological reference Earth model (AuSREM). As a consequence, we produce a model with a high level of detail in both the crust and upper mantle. Our new results strengthen the argument for a low velocity upper mantle anomaly that extends down to ~150 km depth directly beneath the Newer Volcanics Province in Victoria, which is likely related to recent intra-plate volcanism. Beneath Bass Strait, which is thought to host the entrained VanDieland microcontinent, upper mantle velocities are low relative to those typically found beneath Precambrian continental crust; it is possible that failed rifting in Bass Strait during the Cretaceous, opening of the Tasman Sea, extension of VanDieland during Rodinian break-up and recent plume activity in the past 5 Ma may have altered the seismic character of this region. The data nevertheless suggest: (1) the velocity structure of the VanDieland microcontinent lacks continuity within its lithosphere; (2) the Moyston Fault defines an area of strong velocity transition at the boundary between the Cambrian Delamerian Orogen and the Cambrian-Carboniferous Lachlan Orogen; and (3) there is a rapid decrease in mantle velocity inboard of the east coast of Australia, which is consistent with substantial thinning of the lithosphere towards the passive margin.

KEY WORDS: teleseismic tomography, body waves, surface waves, upper mantle, Bass Strait, southeast Australia

1. Introduction

As a result of numerous studies carried out in southeastern Australia (Boger and Miller, 2004; Cawood, 2005; Cayley, 2011; White et al., 2013; Moresi et al., 2014; Pilia et al., 2015a, 2015b; Moore et al., 2015, 2016 - for earlier studies, see references in these publications), knowledge of the geological and tectonic relationship between mainland Australia and Tasmania, which are separated

by Bass Strait, has markedly improved over the past few decades (see Fig. 1 for geological map). However, very little can be inferred about the lower crust and mantle lithosphere from these studies, and consequently, a more complete picture of the region is yet to emerge.

The main difficulties in linking Tasmania and mainland Australia are the presence of Bass Strait, which separates the two land masses, the presence of three thick Cretaceous to recent sedimentary basins (Bass, Gippsland and Otway) and the widespread occurrence of recent intrusive and extrusive volcanism, which have largely prevented direct observation of the underlying basement rocks. Although gravity and magnetic data can provide useful insight into basement structures (Cayley et al., 2011; Moore et al., 2015, 2016), the thickness of the failed-rift sedimentary basins that formed during Australia-Antarctica breakup is a major obstacle for understanding the Proterozoic-Palaeozoic connection between the lithosphere of Tasmania and mainland Australia. To date, most models that attempt to connect Victoria and Tasmania either rely on the interpolation of information between outcrops in both states, with some additional constraints provided by potential field data (e.g. Leaman et al., 1994; Morse et al., 2009), geochemical investigations and seismic reflection profiling (e.g. O'Sullivan et al., 2000; Drummond et al., 2000). One hypothesis that has recently gained significant traction is that a fragment of Precambrian continental lithosphere, set adrift by the break-up of the supercontinent Rodinia, became entrained in the convergent accretionary system responsible for the formation of the Lachlan Orogen, and now underlies both western Tasmania and southern Victoria (Cayley et al., 2002; Direen and Crawford, 2003; Glen, 2005; Cayley et al., 2011; Moresi et al., 2014; Moore et al., 2015, 2016). Ambient noise tomography has also been employed to image crustal structure beneath Bass Strait, with initial results pointing to the possible presence of a Precambrian continental fragment (Pilia et al., 2015a, 2015b). In other studies that are based on stratigraphic and geochemical considerations, Black et al. (2004) found evidence for the presence of Precambrian lithosphere underlying Tasmania and King Island, and Meffre et al. (2004) concluded that the Neoproterozoic mafic volcanics and intrusive sequences of eastern King Island have many geochemical and stratigraphic characteristics that indicate 579 Ma rifting associated with an extensive volcanic passive margin. All these studies focus mainly on the crustal portion of the lithosphere; as such, the inclusion of data capable of constraining the mantle lithosphere has the potential to shed new light on the structure and tectonic evolution of Bass Strait.

In this paper, we apply teleseismic tomography to a dataset recorded by the high density WOMBAT and BASS transportable seismic arrays, which comprise of over 620 stations, deployed during the course of 15 separate array movements. These datasets are combined for the first time to constrain

3-D velocity perturbations in the upper mantle beneath Bass Strait. Teleseismic tomography utilises relative arrival time residuals from distant earthquake sources, recorded across an array of seismic stations, to image the seismic structure of the upper mantle beneath the array. A key assumption is that relative arrival time residuals across the receiver array are largely unaffected by lateral variations in the structure outside a local model volume defined beneath the array. Typically, shallow structure to a depth approximately equal to the station spacing (Rawlinson et al., 2010) is not constrained due to the near-vertical trajectories of impinging teleseismic rays. Here, we address this limitation by incorporating an ambient noise crustal model in our starting model. Another improvement, compared to traditional schemes, is the incorporation of an explicit Moho surface and large-scale mantle velocity variation in the starting model, which are sourced from the AuSREM model of the Australian continent (Kennett and Salmon, 2013).

Teleseismic body wave tomography has been frequently used in various parts of the world (Aki et al., 1977; Oncescu et al., 1984; Humphreys and Clayton, 1990; Achauer, 1994; Steck et al., 1998; Lippitsch et al., 2003; Rawlinson et al., 2006) but has never been applied to study the upper mantle beneath Bass Strait. However, teleseismic tomography studies have been carried out in northern Tasmania (Rawlinson et al., 2006) and southeastern mainland Australia (Graeber et al., 2002; Rawlinson and Kennet, 2008; Rawlinson et al., 2011; Rawlinson and Fishwick, 2012; Rawlinson et al., 2015; Rawlinson et al., 2016), but they have only been able to yield limited insight into the relationship between the two landmasses. The inclusion of the BASS dataset, which spans Bass Strait, together with adjacent data from the mainland and Tasmania, provides a unique opportunity to image this region in detail using seismic techniques.

2. Data and Method

2.1 Teleseismic data

The teleseismic data for this study come from the WOMBAT transportable seismic array deployments between 1998 and 2012 and the recent BASS array, which was deployed from 2011 to 2013 (Fig. 2). Each WOMBAT deployment involves between 20 to 70 stations deployed as a single array, which after 6-12 months is transported to an adjacent location in order to achieve a high density coverage over a large region. The average spacing between WOMBAT stations varies from 15 km in Tasmania to 50 km on the mainland. The seismometers used for this array are either 1 Hz vertical component L4Cs (up until 2006), or 3-component 1Hz Lennartz LE-3Dlites. A number of arrays (e.g. TIGGER and SEAL2) also incorporate several broadband seismometers (Guralp 40T or

3ESP).

In the case of the BASS array, the dataset consists of approximately 23 months (May 2011 to April 2013) of passive seismic data recorded by an array of 24 three-component broadband instruments covering southern Victoria, several islands in Bass Strait (Flinders, King and Deal islands) and northern Tasmania (Fig. 2). The instruments consist of 23 Guralp 40T and one Guralp 3ESP broadband sensors. The 40T instrument has a flat response from 50Hz to 30s period and the 3ESP has a flat response from 50Hz to 60s period. The instruments are connected to Earth Data PR6-24 portable field recorders.

The teleseismic dataset is characterised by dominant source regions to the north and east and a much lower concentration of sources to the west and south of the study area. A total of 53,957 P-wave relative arrival time residuals from 1558 events are used in the teleseismic tomography; since we are using a transportable array (combined total of 624 receivers from 15 sequential deployments), each event is only recorded by the sub-array which was operating at the time that it took place. Teleseismic events with an angular distance >27° (from the centre of each array) and $M_w \geq 5.5$ are considered. Figure 3 shows a plot of the locations of all teleseismic events used in this study.

2.2 Arrival time residual estimation and inversion

The coherence of teleseismic arrivals across dense seismic arrays allows the relative onset times of various global phases to be estimated with high accuracy. In this study, the adaptive stacking scheme of Rawlinson and Kennett (2004) is used to extract residuals from the BASS array. Residuals from the Tasmanian and mainland arrays were extracted using exactly the same procedure described in previous studies (Rawlinson and Urvoy, 2006; Rawlinson et al., 2016). Adaptive stacking exploits the similarity between waveforms to provide a rapid, accurate and robust procedure for estimating the residual patterns across a network of seismic stations. Following any pre-processing of the data (in our case, unifying instrument responses and band pass filtering between 0.3-5.0 Hz), the first step of the scheme involves approximate alignment of all filtered traces according to predictions from a propagation model (ak135), which are then stacked to form a reference trace. Iterative improvement of the alignment, by comparison of the reference trace with each station trace, leads to a direct estimate of the residuals relative to the 1-D propagation model. This technique has proven to be fast and works well in the presence of noisy data and some waveform distortion (Rawlinson and Kennett, 2004). Figure 5 shows an example of adaptive stacking applied to traces from the BASS array experiment.

The arrival time residuals are mapped as 3D perturbations in P-wave velocity with respect to a reference model using teleseismic tomography. The teleseismic tomography method assumes that relative arrival time residuals across the array are largely unaffected by lateral structural variations from outside the local 3-D model volume beneath the array. The software package FMTOMO was used to perform the teleseismic tomography; FMTOMO uses the Fast Marching Method (FMM) (Sethian, 1996; Sethian and Popovici, 1999; Rawlinson and Sambridge, 2004a, 2004b; de Kool et al., 2006) for the forward prediction step and a subspace inversion scheme to adjust model parameters in order to match observed and predicted traveltime residuals subject to damping and smoothing regularisation (Kennett et al., 1988). The method is iterative non-linear in that the inversion step assumes local linearity, but repeated application of FMTOMO and subspace inversion allows the non-linear relationship between velocity and traveltime perturbations to be reconciled (see Rawlinson and Urvoy, 2006, and Rawlinson et al., 2016 for more information on FMTOMO).

2.3 3-D Starting model

2.3.1 Crustal model

In order to mitigate a recognised weakness of teleseismic tomography- its inability to accurately constrain shallow structure to a depth roughly equal to the station spacing (e.g. Rawlinson et al., 2010) - a high resolution crustal model derived from ambient noise data that properly accounts for the crustal contribution to the measured arrival time residuals was included in the starting model for the inversion of WOMBAT and BASS teleseismic arrival time residuals (see supporting information Text S1). As an alternative to the AuSREM crustal velocity model, the crustal model derived from WOMBAT ambient seismic noise data contains well constrained features as small as 30–50 km horizontally and 2–5 km vertically. The robustness of this model is evident from the features recovered (Fig. 4), which share a strong association with the surface geology and constraints provided by potential field data in this region (Leaman et al., 1994; Morse et al., 2009). As such, we believe that it is the better model to use for crustal corrections of the teleseismic traveltime residuals.

2.3.2 Upper mantle model

The AuSREM Moho model (Kennett et al., 2013) and broad scale mantle structure (Figs. 4c and 7 respectively) were also included in the starting model. It is well known that relative arrival time residuals computed for adjacent arrays operating at different times are not directly comparable due to the average velocity structures beneath them likely being different (e.g. Rawlinson et al., 2016).

Hence, unless we incorporate a robust 3-D reference model with a scale length less or equal to the aperture of the smallest seismic array that is used, or have a backbone array of stations that record throughout the durations of the transportable array experiment, then the solution model is likely to contain artifacts, including the loss of long-wavelength structure. In our case, the AuSREM mantle velocity model is sufficiently robust to allow the linking of the different WOMBAT and BASS relative arrival time residual datasets in a joint inversion.

Seismic data exploited by AuSREM comes from over 12,000 km of deep crustal reflection profiles, a number of major refraction experiments, and many different passive seismic deployments (Kennett et al., 2013, Salmon et al., 2013). Due to moderate coverage of reflection data in this region and constraints from receiver functions, the broadscale variations in AuSREM Moho geometry are likely to be reasonably robust. However, this is not true for crustal P-wave velocity, which is only constrained by a few 2-D refraction experiments in the model region (Salmon et al., 2013); hence our use of an ambient noise crustal model in the 3-D starting model.

2.4 Conversion of S to P velocity

One limitation of the ambient noise model used for crustal correction is that it defines S-wave velocities, whereas the teleseismic arrival time residuals come from global P-phases. We cannot use S-phases in this study because the majority of WOMBAT stations are short period (~1 Hz corner frequency), which makes teleseismic S-arrivals difficult to detect in comparison to P. In order to convert from S-wave velocity to P-wave velocity, we apply the same approach as Rawlinson et al. (2016), who use the AuSREM crustal Vp/Vs model (Salmon et al., 2013); although it features lower lateral resolution compared to our new lithospheric model, the peak Vp/Vs perturbations are only around ~3% which are unlikely to be a factor in the correction of P-wave arrival time residuals for crustal structure.

3. Results

We represent the seismic structure of the southeast Australian lithosphere using a two-layer model consisting of a crust and upper mantle separated by a Moho surface. Compared to previous teleseismic studies that exploit WOMBAT data to image the lithosphere beneath southeast Australia (Graeber et al., 2002; Rawlinson et al., 2006, 2011; Clifford et al., 2008; Rawlinson and Kennett, 2008; Fishwick and Rawlinson, 2012; Rawlinson et al., 2015, 2016), the work presented here uses a geographically more extensive dataset that also covers Bass Strait and northern Tasmania. However, the broad-scale variations in wave speed in regions that overlap with previous studies are

in general agreement; this is a reassuring sign when sequential studies are performed in the same region using increasingly large datasets and/or different tomographic imaging schemes (Fishwick and Rawlinson, 2012).

The inversion result was obtained by using six iterations of FMTOMO, with a starting model defined by 459,000 velocity nodes and 7650 interface nodes. The data misfit component of the objective function is based on the difference between observed residuals and model residuals. In the latter case, these residuals are computed by taking the difference between predictions through the recovered model (with receivers set at the correct elevation) at each iteration and ak135 reference model predictions (with receivers set to zero elevation). Therefore, contributions to the predicted residual from crustal velocity, Moho geometry and long wavelength mantle structure is accounted for, as is the fact that adaptive stacking residuals were calculated using move-out corrections under the assumption that all receivers were at the same elevation. It is important to note, therefore, that the starting model for the inversion, which contains lateral structure in the crust, mantle and Moho, is not the same as the laterally invariant model used to compute the reference arrival times. In order to produce a model that does not greatly deviate from the starting model and contains no unnecessary features, while at the same time having an acceptable fit to the data, damping and smoothing values are chosen using the approach of Rawlinson et al. (2006) which is based on a three step procedure using trade-off curves between data variance and model variance, and data variance and model roughness (Fig. 6). This involves running a series of inversions with different levels of damping and smoothing in order to identify the model with minimum perturbation and roughness that still satisfies the data to an acceptable level. If we assume that the point of maximum curvature on the trade-off curve provides the optimum compromise, then both the damping and smoothing values are ~200 in our case (Fig. 6). However, it is well known that this approach is ad-hoc, and following extensive testing, we ultimately prefer to use the same damping and smoothing (75 in both cases) as Rawlinson et al. (2016) which produces a slightly underdamped and undersmoothed version of the optimum model (according to the trade-off curves). We believe that this model reveals features that are more consistent with crustal structure (from ambient noise tomography) and broadscale surface geology. However, the differences between the two models are not large, with our preferred model exhibiting a very similar pattern of anomalies, albiet with slightly larger amplitude (see Supplementary Figs. S1-S3 for models produced using various damping and smoothing values, including the “optimum” model according to the trade-off curves). The final solution model, based on damping and smoothing values of 75, resulted in a variance reduction in the traveltime residual misfit of 73% relative to the starting 3-D model (and 78% relative to ak135). Below, we present the results of a synthetic recovery test and the solution model

for mantle P-wave velocities.

3.1 Synthetic test

Because of solution non-uniqueness in seismic tomography problems a single data-satisfying model may contain features that are not required by the data. Therefore, before interpreting our solution model, the robustness of the data constraints is first investigated using a synthetic checkerboard test (Glahn and Granet, 1993; Ritsema et al., 1998; Day et al., 2001; Rawlinson and Sambridge, 2003; Rawlinson and Kenneth, 2008). This test involves using the identical sources, receivers and phase types from the observational dataset to predict the arrival time-residuals for a synthetic structure comprising an alternating 3D pattern of fast and slow velocities, separated by a narrow region of zero perturbation (Fig. 8a and c). Here, we are only testing the resolving power of the teleseismic dataset, because the crustal velocities are derived from ambient noise tomography alone and have no dependence on the mantle velocities or teleseismic data. Hence, velocity anomalies are only imposed on upper mantle structure, and both crustal velocity variations and the AuSREM Moho are held fixed.

Prior to running an inversion for recovery of the synthetic checkerboard, Gaussian noise with a standard deviation of 59 ms was added to the synthetic dataset. This is equal to the standard deviation of the noise estimated by the adaptive stacking procedure used to extract the relative arrival time residuals. The predicted data are then inverted using the same tomographic procedure that is applied to the observations, including the same damping and smoothing values. Following the inversion, the difference between the input and output models can be used as a measure of how well structure can be recovered (Fig. 8b and d). This test is often favoured in seismic tomography (e.g. Graeber and Asch, 1999; Rawlinson et al., 2011) because a continuous pattern makes interpretation relatively straight forward; however, it cannot be regarded as a comprehensive test of solution robustness (Lévêque et al., 1993; Rawlinson and Spakman, 2016).

The east – west cross-sections through the checkerboard inversion model (Fig. 9(A-A')) generally exhibit good recovery, although there is some smearing of structure towards the edge of the array caused by a predominance of paths with similar orientations. The north – south cross-sections (Fig. 9(B-B')) also recover some of the checkerboard pattern, although smearing is clearly evident beyond the horizontal bounds of the array. The smearing is dominant in the north-south direction as a consequence of source distribution which results in many more paths impinging on the model from the north compared to the south. Similarly, the centre of Bass Strait is poorly recovered at shallow depth, which can be attributed to an absence of receivers (such as ocean bottom

seismometers) in the marine environment. The minimum scale length of structure that can be recovered by teleseismic tomography is typically equal to the station spacing (Rawlinson et al., 2015), which in this case is around 50 km, similar to the mainland station spacing. In summary, the upper mantle structure appears to be well constrained by the path coverage, although resolution tends to decrease beyond the horizontal bounds of the seismic array (see Supplementary Fig. S4 for additional checkerboard recovery tests).

3.2 WOMBAT-BASS model

The model recovered from inversion of WOMBAT and BASS teleseismic datasets is shown in Figures 10, 11 and 12 (note that the grey mask denotes less resolved areas as determined by inspection of checkerboard test results), and reveals a number of significant structural features. The horizontal slice at 75 km depth (Fig. 10) shows an E-W (latitude 37.2° S) trending low velocity anomaly in the upper mantle in southern Victoria (see dashed rectangle SV), which lies to the north of a narrow high velocity anomaly located along the SE Victorian coast. Bass Strait appears as a relatively low velocity zone (noting that it is not well resolved in the centre at this depth) while upper mantle velocities in northern Tasmania vary from fast to slow to fast from west to east (see dashed rectangle NT in Fig. 10). North of the line A-A' in Figure 10, the model is largely consistent with the body wave tomography model of Rawlinson et al. (2016), which uses the same mainland arrival time residual dataset from WOMBAT. At greater depths beneath the southern region of the model, the pattern of velocity anomalies becomes less coherent, but the lower velocities beneath southern Victoria and Bass Strait and the higher velocities to the north extend to well over 100 km depth (B-B' in Fig. 11). In general, the pattern of residuals in the crust and Moho variations do not appear to share an overall anti-correlation with uppermost mantle anomalies, which at least suggests that crustal structure is not dictating upper mantle structure.

In order to reinforce the importance of a 3-D starting model in improving the recovery of mantle structure, a comparative test was carried out. Here, the inversion of the data was carried out using a purely 1-D starting model (ak135) in the crust and upper mantle, and a flat Moho consistent with ak135. The recovered model in Figure 13 shows clear similarities and differences with the solution produced using a 3-D starting model (Fig. 12). The lack of longer wavelength structures in Figure 13, particularly evident in the cross-sections, would make interpretation more challenging if this model was considered in isolation. Furthermore, while there is general agreement on the shorter wavelength structures, there are differences evident, particularly at shallow mantle depths. Of particular relevance to this study is the presence of high velocity anomalies appearing to connect Tasmania and Victoria across Bass Strait in the 75 km and 120 km depth slices of Figure 13. This

may lead one to conclude that the two share a structural connection in the mantle lithosphere, but as Figure 12 demonstrates, these anomalies are more likely to be artifacts caused by the vertical smearing of unresolved crustal structure.

4. Discussion

The inversion of the WOMBAT-BASS dataset has produced a high resolution lithospheric velocity model of Bass Strait and adjoining southeast mainland Australia and Tasmania. Many intriguing features are observed in our P-wave velocity model that could pertain to tectonic processes that affected the study area. Several velocity anomalies imaged in our study are present in previously determined models of northern Tasmania and southern Victoria. These include the high velocities found in the upper mantle beneath the Rocky Cape Block of north-west Tasmania (Rawlinson and Urvoy, 2006; Rawlinson and Kennett, 2008) and regions of low mantle velocity beneath the Tamar Fracture System (TFS) and Newer Volcanics Province (NVP) (Rawlinson and Fishwick, 2012; Rawlinson et al., 2015; Rawlinson et al., 2016). Further north, higher velocities associated with cratonic regions and lower velocities near the eastern seaboard, which are likely due to lithospheric thinning towards the passive margin, can be observed (Rawlinson et al., 2016). A recent study that also shows consistency with our results in terms of lower velocities underneath the Lachlan Fold Belt and Bass Strait is that of Sun et al. (2016). In their study, they apply 3-D P_n travel time tomography to improve structural constraints on the uppermost mantle across the Australian continent. They find some of the lowest velocities beneath the southern Lachlan Fold Belt, the Newer Volcanics province and Bass Strait, which largely agrees with our teleseismic body wave tomography model, and supports the idea that recent intraplate volcanism, coupled with lithospheric thinning associated with failed rifting, have strongly influenced the seismic structure of the lithosphere in this region.

Our new tomographic model exhibits a distinct north dipping low velocity anomaly that extends from just below the crust to ~150 km depth in the upper mantle directly beneath the NVP (see Fig. 12 cross-section A-A'). Previously, Davies et al. (2015) identify the world's longest continental hot-spot track (over 2000 km total length), which begins in north Queensland, and extends southward, possibly as far as NW Tasmania. Their study suggests that the plume source of the hotspot track passed by the eastern edge of the NVP shortly before volcanism initiated nearly 5 Ma. In another study, Rawlinson et al. (2017) suggest that an interaction between this passing plume and pre-existing Edge Driven Convection (EDC) (King and Anderson, 1998) and Shear Driven Upwelling (SDU) (King and Ritsema, 2000) (caused by a huge central cavity in the lithosphere, which corresponds to the central low velocity zone north of the NVP in our model) was responsible for the

NVP volcanism. A more recent study by Wei et al. (2018) using 3-D S_n traveltime tomography finds strong heterogeneities in S wave speed in the upper mantle across the entire Australian continent. They also include Pn data to determine the uppermost mantle Vp/Vs ratio across the whole continent. Their study finds distinctive localised low velocity anomalies beneath the eastern margin of Australia which they interpret as evidence of mantle plume remnants. Our model shows a low velocity zone beneath Bass Strait (Fig. 12 cross-section C-C'), but below 200 km depth these lower velocities disappear entirely. A recent study has suggested that the plume was waning as Australia gradually moved north (Jones and Verdel, 2015), so it is possible that there is no longer any clear evidence for it at greater depth. Nonetheless, it may have contributed to the lower velocities observed beneath Bass Strait.

Our seismic tomography results appear to be consistent with the findings of previous studies regarding the boundary between the Lachlan and Delamerian Orogens (Rawlinson et al., 2015; Rawlinson et al., 2016). The mantle model of Rawlinson et al. (2016), which covers mainland southeast Australia, shows a clear transition from high velocities in the west to lower velocities in the east. This same velocity transition is clearly imaged in our model (Fig. 11). Moreover, the location and dip direction of the velocity transition (marked "DLB" in section B–B′ of Fig. 12) is consistent with the Moyston Fault at the surface (Cayley and Taylor, 1998; VandenBerg, 1999; Cayley et al., 2002), which is a widely accepted candidate for the Delamerian–Lachlan boundary in the crust. However, while the velocity transition in the mantle is unlikely to represent a continuation of this fault, it may be the signature of an W-E contrast from Precambrian to Palaeozoic mantle lithosphere.

A long standing source of debate in southeast Australian tectonics is the possible connection between the mainland Delamerian Orogen and the Tyennan Orogen in Tasmania, where there have been two schools of thought. Crawford et al. (2003) and Reed et al. (2002) proposed a model depicting the two orogens connected directly. This connection is reinforced by several studies that have examined the age and geochemistry of various igneous rocks in both regions, and found strong similarities. For example, Direen and Crawford (2003), have found paired suites of unusual ~580 Ma olivine rich mafic volcanics, together with rare ~515 Ma boninites in both western Victoria and the mainland Delamerian Orogen. However, subsequent studies (e.g. Cayley et al., 2011; Moore et al., 2015, 2016) argued that the two orogens are not connected directly. In particular, Moore et al. (2015) found that the Tyennan and Delamerian Orogenies occurred at the same time but are displaced along strike. In their model, the Tyennan Orogeny takes place further to the east and is controlled by the master subduction zone to the Pacific plate.

In light of the above discussion, it is interesting to note that the velocity transition “DLB” observed on the mainland does not show any extension southwards through Bass Strait to Tasmania. However, one of the challenges in trying to interpret structure that was emplaced in the distant past from present day geophysical images is that subsequent deformation and alteration will mask pre-existing features and make any meaningful interpretation difficult. Notable tectonic events that post-date the formation of the Delamerian and Lachlan Orogens include the break-up of Australia and Antarctica and opening of the Tasman Sea, which resulted in the formation of the associated failed rift basins that accommodate thick sedimentary sequences (Gaina et al., 1998). These events also resulted in substantial thinning of the lithosphere towards the passive margin. The lower velocities observed beneath the Bass Strait-Tasmania region (Fig. 12 cross-section C-C'), may be a result of elevated temperatures associated with the rifting and the presence of a thinner lithosphere, as well as the influence of the plume associated with the Cosgrove track. Hence the interpretation of Cayley et al. (2011) and Moore et al. (2015, 2016) may be consistent with our observation of the DLB not extending south into Bass Strait, implying no direct connection between the Delamerian and Tyennan Orogens.

Recent studies have strengthened the argument for the presence of a Proterozoic continental fragment, sourced from the break-up of Rodinia, beneath the Melbourne Zone in southern Victoria (the so-called Selwyn Block), which extends south through Bass Strait to form the Precambrian basement of western Tasmania (Cayley, 2011; Moresi et al., 2014; Pilia et al., 2015a, 2015b; Moore et al., 2015, 2016). Following the earlier work of Cayley (2011), the existence of an entrained Precambrian continental fragment has been reinforced by using 3-D geodynamic modeling (Moresi et al., 2014). This study suggests that an exotic continental fragment became entrained in the proto-Pacific convergent margin of eastern Australia, which resulted in a complex sequence of processes including differential subduction roll-back and southward transfer of material through continental transform faulting to form a large orocline that now underlies the Lachlan Orogen. The models illustrate how significant curvature of the orogenic system develops, as well as the mechanism for tectonic escape of the back arc region.

Moore et al. (2015, 2016) provide robust geological and potential field evidence for the processes that led to the formation of Tasmania and how it is connected to mainland Australia. Their studies suggest that an extensional event along the Proto-Terra Australis margin began Rodinian breakup at approximately 830 Ma. As the extension continued, rifting took place along the Rodinian margin at around 600 Ma, which resulted in the separation of Laurentia, leaving vanDieland (comprising of the Selwyn Block, western Tasmania and the western part of the Bass Strait) attached to a thinned Gondwana margin. By 580 Ma vanDieland was completely rifted from Rodinia, forming three or

four weakly connected cratonic ribbons separated by thinned continental or back-arc oceanic crust and a completely detached King Island. At the beginning of Ross Orogeny subduction, the rifted fragments of vanDieland drifted northwards at approximately 560 Ma. By 510 Ma or shortly thereafter, trench advance during the Tyennan Orogeny caused closure between the cratonic blocks bringing most of them together. Finally, the micro continental ribbons became accreted within a closing back arc system and later, together with eastern Tasmania and the Lachlan Orogen, coalesced with the Gondwana Craton in the Middle Devonian. By 495 Ma all subduction processes had stalled and post collisional extension was underway. Moore et al. (2015, 2016) also demonstrate how the accreted vanDieland ribbons can be traced from present day Tasmania across Bass Strait into the Selwyn Block, thereby providing evidence that vanDieland is embedded in the Lachlan Orogen in southeast mainland Australia.

Pilia et al. (2015a) studied Bass Strait and adjoining land masses by applying a transdimensional Bayesian inversion scheme to WOMBAT and BASS data to retrieve group velocity maps and 3-D shear wavespeed. The result is an image of the entire crust beneath Bass Strait that reveals a high velocity anomaly connecting southern Victoria and western Tasmania in the mid-lower crust, which is suggestive of a Proterozoic geological connection. This high velocity anomaly is consistent with recent gravity and magnetic maps and results from a seismic reflection survey through the Melbourne Zone in southern Victoria (Cayley et al., 2002, Cayley et al., 2011).

Our new model shows that high velocity anomalies in the upper mantle tend to underlie crust of Precambrian continental origin, for example the Curnamona Province and Gawler Craton in Figure 12. Contrary to this, apart from the narrow sliver beneath the Melbourne zone, there is no evidence of a high velocity body in the upper mantle connecting mainland Australia and Tasmania. However, as noted previously, this does not necessarily rule out the existence of Precambrian continental material. Apart from the influence of recent plume activity, two possible explanations include delamination of the mantle lithosphere beneath the fragment triggered by edge driven convection and shear driven upwelling (Rawlinson et al., 2017), or so-called rift-induced delamination (Wallner and Schmeling, 2010). Interestingly, mantle velocities below 200 km depth beneath Bass Strait (Fig. 12, cross-section C-C') are anomalously high compared with mantle beneath the Australian mainland, which potentially supports this hypothesis. However, the lack of any apparent uplift in Bass Strait, which would normally be a required response to the loss of a dense lithospheric mantle layer, means that this is not very likely. Furthermore, the deep high velocity zone is in part inherited from AuSREM (Fig. 7d), which may not be well constrained in this region. A third possible explanation is that the micro-continent was subjected to intense lithospheric rifting during 250 Myr of Neoproterozoic extension which lead to Rodinian break-up,

as suggested by Moore et al. (2015). This resulted in the development of continental ribbons (boudins), which by 510 Ma or shortly thereafter were brought together by the Tyennan Orogeny. This Rodinian extension is likely to have modified and thinned any high velocity mantle, resulting in a similar velocity signature to present day rifted margins.

Previous studies (e.g. Pilia et al., 2015a, Rawlinson et al., 2016) have also suggested that any high velocity associated with a lithospheric keel beneath an entrained Precambrian continental fragment may have been overprinted by failed rifting associated with the break-up of Australia and Antarctica and the opening of the Tasman Sea between 80 and 90 Ma (Gaina et al., 1998). Both of these events would have resulted in substantial thinning of the lithosphere in the Bass Strait region (marked 'BS' in Fig. 12, cross-section C-C'), and potentially elevated upper mantle temperatures. The rapid eastward decrease in upper mantle velocities towards the east coast of Australia (marked 'LTZ' Fig. 12) is consistent with lithospheric thinning associated with the opening of the Tasman Sea. This change is due to the proximity of the passive margin and may be accentuated by the presence of asymmetric rifting, with the upper-plate margin underlying the Australian east coast (Lister et al., 1986; Lister and Etheridge, 1989; Lister et al., 1991).

5. Conclusions

In this study, a P-wave velocity model of the crust and upper mantle was used to investigate the broad-scale geology of the Bass Strait region. The inversion of teleseismic arrival time residuals from WOMBAT and BASS transportable array data for mantle velocity variations was improved by embedding a detailed ambient noise crustal model and AuSREM Moho and mantle velocity variations in the starting model. Resolution tests show that the new model of the Bass Strait region is generally well constrained by the data set beneath the horizontal bounds of the array, although there is a lack of coverage beneath the centre of Bass Strait to a depth of approximately 100 km due to the use of only land-based stations. North of Victoria, the pattern of anomalies is consistent with previous studies that have exploited the WOMBAT teleseismic dataset. We also image a distinct low velocity zone beneath the NVP in western Victoria, and show that (i) it is restricted to the upper mantle, and appears to die out at around 150 km depth; and (ii) it lies at the northern end of a pervasive low velocity zone in the upper mantle that stretches between Victoria and Tasmania. As such, we do not find any evidence to support the existence of a Precambrian microcontinent that joins Tasmania to the mainland, as has been suggested in recent studies. However, we cannot rule out the possibility that hyper-extension during Rodinian break-up, failed rifting in Bass Strait associated with the separation of Australia and Antarctica, the opening of the Tasman Sea and mantle sources of recent intra-plate volcanism may have conspired to reduce seismic wavespeeds

via processes such as lithospheric stretching, delamination, changes in bulk composition and heating.

Acknowledgments

We thank many land owners and field team members from mainland Australia and Tasmania. Particular thanks to Armando Arcidiaco and Qi Li from ANU for assistance with the collection and archiving of the data used in this study. ARC grants DP120103673, LE120100061, LP110100256 and DP0986750 were instrumental in supporting the WOMBAT and BASS deployments.

References

Achauer, U., 1994. New ideas on the Kenya rift based on the inversion of the combined dataset of the 1985 and 1989/90 seismic tomography experiments. Tectonophysics 236, 305 – 329.

Aki, K., Christossffersson A., Husebye, E. S., 1977. Determination of the three dimensional seismic structure of the lithosphere. J. Geophys. Res. 82, 277–296.

Benson, G. D., Ritzwoller, M. H., Shapiro, N. M., 2008. Broadband ambient noise surface wave tomography across the United States. J. Geophys. Res. 113, http://dx.doi.org/ 10.1029/2007JB005248.

Black, L.P., Calver, C.R., Seymour, D.B., Reed, A., 2004. SHRIMP U-Pb detrital zircon ages from Proterozoic and Early Palaeozoic sandstones and their bearing on the early geological evolution of Tasmania. Australian Journal of Earth Sciences 51, 885-900.

Boger, S., and Miller, J., 2004.Terminal suturing of Gondwana and the onset of the Ross Delamerian Orogeny: the cause and effect of an Early Cambrian reconfiguration of plate motions. Earth and Planetary Science Letters 219, 35–48.

Cawood, P.A., 2005.Terra Australis Orogen: Rodinia breakup and development of the Pacific and Iapetus margins of Gondwana during the Neoproterozoic and Paleozoic. Earth-Science Reviews 69, 249–279. http://dx.doi.org/ 10.1016/j.earscirev.2004.09.001.

Cayley, R. A., Taylor, D. H., 1998. The Lachlan margin Victoria: the Moyston Fault, a newly recognised terrane boundary. Geol. Soc. Aust. Abstr. 49, 73.

Cayley, R., Taylor, D. H., VandenBerg, A. H. M., Moore, D. H., 2002. Proterozoic–Early Palaeozoic rocks and the Tyennan Orogeny in central Victoria: the Selwyn Block and its tectonic implications. Aust. J. Earth Sci. 49, 225–254.

Cayley, R., 2011. Exotic crustal block accretion to the eastern Gondwanaland margin in the Late Cambrian Tasmania, the Selwyn Block, and implications for the Cambrian–Silurian evolution of the Ross, Delamerian, and Lachlan orogens. Gondwana Research 19, 628–649. http://dx.doi.org/10.1016/j.gr.2010.11.013.

Cayley, R., Korsch, R. J., Moore, D. H., Costelloe, R.D., Nakamura, A., Willman, C. E., Rawlin, T. J., Morand, V. J., Skladzien, P. B., O'Shea, P. J., 2011. Crustal architecture of central Victoria: results from the 2006 deep crustal reflection seismic survey. Australian Journal of Earth Sciences 59, 113-156.

Clifford, P., Greenhalgh, S., Houseman, G., Graeber, F., 2008. 3-d seismic tomography of the Adelaide fold belt, Geophys. J. Int. 172, 167–186.

Crowder, E., Rawlinson, N., Pilia, S., Cornwell, D. G. and Reading, A. M., 2019. Transdimensional ambient noise tomography of Bass Strait, southeast Australia, reveals the sedimentary basin and deep crustal structure beneath a failed continental rift. Geophysical Journal International, 217, 970-987.

Crawford, A. J., Meffre, S., and Symonds, P. A., 2003. 120 to 0 Ma tectonic evolution of the southwest Pacific and analogous geological evolution of the 600 to 220 Ma Tasman Fold Belt System. In: Hillis R. R. & Mülle R. D. eds. Evolution and dynamics of the Australian Plate, 383–404. Geological Society of Australia Special Publication 22 and Geological Society of America Special Publicaion 372.

Dalton, C. A., Faul, U. H., 2010. The oceanic and cratonic upper mantle: clues from joint interpretation of global velocity and attenuation models. Lithos 120, 160–172.

Davies, D. R., Rawlinson, N., Iaffaldano, N., Campbell, I. H., 2015. Lithospheric controls on magma composition along Earth's longest continental hotspot track. Nature 525, 511–514.

Day, A. J., Peirce, C., Sinha, M. C., 2001. Three-dimensional crustal structure and magma chamber geometry at the intermediate spreading, back-arc Valu Fa Ridge, Lau Basin—results of a wide-angle seismic tomographic inversion. Geophysical J. Int. 146, 31–52.

de Kool, M, Rawlinson, N., Sambridge, M., 2006. A practical grid based method for tracking multiple refraction and reflection phases in 3D heterogeneous media. Geophysical J. Int. 167, 253–270.

Direen, N. G., Crawford, A.J., 2003. The Tasman Line: where is it, what is it, and is it Australia's Rodinian breakup boundary? Aust. J. Earth Sci. 50, 491–502.

Drummond, B., Barton, T., Korsch, R., Rawlinson, N., Yeates, A., Collins, C., Brown, A., 2000. Evidence for crustal extension and inversion in eastern Tasmania, Australia, during the Neoproterozoic and Early Palaeozoic. Tectonophysics 329, 1–21. http://dx.doi. org/10.1016/S0040-1951(00)00185-2.

Fishwick, S., Rawlinson, N., 2012. 3-D structure of the Australian lithosphere from evolving seismic datasets. Aust. J. Earth Sci. 59, 809–826.

Gaina, C., Müller, D., Royer, J. -Y., Stock, J., Hardebeck, J., Symonds, P., 1998. The tectonic history of the Tasman Sea, a puzzle with 13 pieces. J. Geophys. Res. 103, 12,413–12,433.

Glahn, A., and Granet, M., 1993. Southern Rhine Graben: small wavelength tomographic study and implications for the dynamic evolution of the graben, Geophys. J. Int. 113, 399–418.

Glen, R. A., 2005. The Tasmanides of Eastern Australia. In: Vaughan, A. P. M., Leat, P.T., Pankhurst, R.J. (Eds.), Terrane Processes at the Margins of Gondwana. Geological Society, London, 23–96.

Graeber, F. M. and Asch, G., 1999. Three-dimensional models of P wave velocity and P-to-S velocity ratio in the southern central Andes by simultaneous inversion of local earthquake data: J. Geophys. Res. 104, 20,237–20,256.

Graeber, F. M., Houseman, G.A., Greenhalgh, S.A., 2002. Regional teleseismic tomography of the western Lachlan Orogen and the Newer Volcanics Province, southeast Australia. Geophysical Journal International 149, 249–266.

Hand, M., Reid, A., Szpunar, M., Direen, N., Wade, B., Payne, J., Barovich, K., 2008. Crustal architecture during the early Mesoproterozoic Hiltaba-related mineralisation event: are the

565 Gawler Range Volcanics a foreland basin fill? MESA J. 51, 19–24.

566 Humphreys, E. D., and Clayton, R. W., 1990. Tomographic image of the southern California
567 mantle. J. Geophys. Res. 95, 19,725 – 19,746.
568
569 Jones, I., and Verdel, C., 2015. Basalt distribution and volume estimates of Cenozoic volcanism in
570 the Bowen Basin region of eastern Australia: Implications for a waning mantle plume.
571 Australian Journal of Earth Sciences 62:2, 255-263, doi: 10.1080/08120099.2015.997796.
572
573 Kennett, B. L. N., Sambridge, M. S., Williamson, P. R., 1988. Subspace methods for large scale
574 inverse problems involving multiple parameter classes. Geophysical. J. Int. 94, 237–247.
575
576 Kennett B. L. N., Fichtner, A., Fishwick, S., Yoshizawa, K., 2013. Australian seismological
577 reference model (AuSREM): mantle component. Geophys J. Int. 192, 871–887.

578 King, S. D., and Anderson, D. L., 1998. Edge-Driven Convection. Earth Planet. Sci. Lett. 160, 289-
579 296.

580 King, S. D., and Ritsema, J., 2000. African hotspot volcanism: small-scale convection in the upper
581 mantle beneath cratons, Science 290, 1137-1140.

582 Leaman, D., Baillie, P., Powell, C.M., 1994. Precambrian Tasmania: a thin-skinned devil.
583 Exploration Geophysics 25, 19–23. http://dx.doi.org/10.1071/EG994019.

584 Lévêque, J. J., Rivern, L., and Wittlinger, G., 1993. On the use of the checkerboard test to assess the
585 resolution of tomographic inversions. Geophys. J. Int. 115, 313 – 318.
586
587 Lippitsch, R., Kissling, E. and Ansorge, J., 2003. Upper mantle structure beneath the Alpine orogen
588 from high-resolution teleseismic tomography. J. Geophys. Res. 108(B8), 2376,
589 doi:10.1029/2002JB002016.
590
591 Lister, G. S., Ethridge, M. A., Symonds, P. A., 1986. Detachment faulting and the evolution of
592 passive continental margins: Geology 14, 246–250.

593 Lister, G. S., Etheridge, M. A., 1989. Detachment models for uplift and volcanism in the Eastern
594 Highlands, and their application to the origin of passive margin mountains. In: Johnson, R.W.
595 (Ed.), Intraplate Volcanism in Eastern Australia and New Zealand. Cambridge University Press,

New York, 297–312.

Lister, G. S., Ethridge, M. A., Symonds, P. A., 1991. Detachment models for the formation of passive continental margins. Tectonics 10, 1038–1064.

Meffre, S., Direen, N.G., Crawford, A. J., Kamenetsky, V. 2004. Mafic volcanic rocks on King Island, Tasmania: Evidence for 579 Ma break-up in east Gondwana. Precambrian Research 135, 177-191.

Moore, D.H., Betts, P.G. & Hall, M., 2015. "Fragmented Tasmania: the transition from Rodinia to Gondwana", Australian Journal of Earth Sciences 62, 1-35.

Moore, D.H., Betts, P.G. & Hall, M., 2016. Constraining the VanDieland microcontinent at the edge of East Gondwana, Australia. Tectonophysics 687, 158-179.

Moresi, L., Betts, P. G., Miller, M. S., Cayley, R. A., 2014. Dynamics of continental accretion. Nature 508, 245–248.

Morse, M., Gibson, G., Mitchell, C., 2009. Basement constraints on offshore basin architecture as determined by new aeromagnetic data acquired over Bass Strait and western margin of Tasmania. ASEG Extended Abstracts 2009, 1–9, http://dx.doi.org/10.1071/ASEG2009ab042.

Oncescu, M. C., Burlacu, V., Anghel, M., Smalbergher, V., 1984, Three-dimensional P-wave velocity image under the Carpathian Arc. Tectonophysics 106, 305–319.

O'Sullivan, P., Mitchell, M., O'Sullivan, A., Kohn, B., Gleadow, A., 2000. Thermotectonic history of the Bassian Rise, Australia: Implications for the breakup of eastern Gondwana along Australia's southeastern margins. Earth and Planetary Science Letters 182, 31–47. http://dx.doi.org/10.1016/S0012-821X(00)00232-6.

Pilia, S., Rawlinson, N., Green, N. G., Reading, A. M., Cayley, R., Pryer, L., Arroucau, P., and Duffet, M., 2015a. Linking mainland Australia and Tasmania using ambient seismic noise tomography: Implications for the tectonic evolution of the east Gondawana margin. Gondwana Research 28, 1212-1227.

Pilia, S., Rawlinson, N., Cayley, R. A., Musgrave, R., Reading, A. M., Direen, N. G., Young, M. K., 2015b. Evidence of micro-continent entrainment during crustal accretion. Sci. Rep. 5. http://dx.doi.org/10.1038/srep/08218.

Rawlinson, N. and Sambridge, M., 2003. Irregular interface parameterization in 3-D wide-angle

seismic traveltime tomography. Geophysical Journal International 155, 79-92.

Rawlinson, N. and Kennett, B. L. N., 2004. Rapid estimation of relative and absolute delay times across a network by adaptive stacking. Geophysical Journal International 157, 332-340.

Rawlinson N, and Sambridge M., 2004a. Multiple reflection and transmission phases in complex layered media using a multistage fast marching method. Geophysics 69,1338–1350.

Rawlinson, N., and Sambridge, M., 2004b. Wavefront evolution in strongly heterogeneous layered media using the fast marching method. Geophysical Journal International 156, 631–647.

Rawlinson, N., Reading, A., Kennett, B., 2006. Lithospheric structure of Tasmania from a novel form of teleseismic tomography: Journal of Geophysical Research 111, B02301. http://dx.doi.org/10.1029/2005JB003803

Rawlinson, N., Urvoy, M., 2006. Simultaneous inversion of active and passive source datasets for 3-D seismic structure with application to Tasmania. Geophys. Res. Lett. 33, L24313.

Rawlinson, N., Kennett, B., 2008. Teleseismic tomography of the upper mantle beneath the southern Lachlan Orogen, Australia. Physics of the Earth and Planetary Interiors 167, 84–97. http://dx.doi.org/10.1016/j.pepi2008.02.07.

Rawlinson, N., Pozgay, S., Fishwick, S., 2010. Seismic tomography: a window into deep Earth. Phys. Earth Planet. Inter. 178, 101–135.

Rawlinson, N., Kennett, B., Vanacore, E., Glen, R., Fishwick, S., 2011. The structure of the upper mantle beneath the Delamerian and Lachlan orogens from simultaneous inversion of multiple teleseismic datasets. Gondwana Res. 19, 788–799.

Rawlinson, N., Fishwick, S., 2012. Seismic structure of the southeast Australian lithosphere from surface and body wave tomography. Tectonophysics 572, 111–122.

Rawlinson, N., Kennett, B. L. N., Salmon, M., Glen, R. A., 2015. Origin of lateral heterogeneities in the upper mantle beneath South-East Australia from seismic tomography. In: Khan, A., Deschamps, F. (Eds.), The Earth's Heterogeneous Mantle: A Geophysical, Geodynamical and Geochemical Perspective, Springer Geophysics. Springer, 47–78.

Rawlinson, N., Pilia, S., Young, M. Salmon, M., Yang, Y., 2016. Crust and upper mantle structure

655 beneath southeast Australia from ambient noise and teleseismic tomography. Tectonophysics
656 689, 143-156. http://dx.doi.org/10.1016/j.tecto.2015.11.034.

657 Rawlinson, N., Spakman, W., 2016. On the use of sensitivity test in seismic tomography. Geophys.
658 J. Int. 205, 1221–1243.

659 Rawlinson, N., Davies, D. R., Pilia, S., 2017. The mechanisms underpinning Cenozoic intraplate
660 volcanism in eastern Australia. Insights from seismic tomography and geodynamic modeling.
661 Geophysical Research Letters 44 (19), 9,681-9,690.
662
663 Reed A. R., Calvert C., Bottrill, R. S., 2002. Palaeozoic suturing of eastern and western Tasmania
664 in the west Tamar region: Implications for the tectonic evolution of southeast Australia.
665 Australian Journal of Earth Sciences 49, 809–830.

666 Ritsema, J., A. Nyblade, A., Owens, T. J., Langston, C. A., VanDecar, J. C., 1998. Upper mantle
667 seismic velocity structure beneath Tanzania, east Africa: Implications for the stability of cratonic
668 lithosphere. J. Geophys. Res. 103, 21201–21213.

669 Salmon, K., Kennett, B. L. N., Saygin, E., 2013. Australian Seismological Reference Model
670 (AuSREM): crustal component. Geophys. J. Int. 192, 190–206.

671 Sethian, J. A., 1996. A fast marching level set method for monotonically advancing fronts. Proc.
672 Natl. Acad. Sci. 93, 1591–1595.
673 Sethian, J. A., and Popovici, A. M., 1999. 3-D traveltime computation using the fast marching
674 method. Geophysics 64, 516 – 523.
675
676 Steck, L. K., Thurber, C. H., Fehler, M., Lutter, W. J., Roberts, P. M., Baldridge, W. S., Stafford, D.
677 G., and Sessions, R., 1998. Crust and upper mantle P wave velocity structure beneath Valles
678 caldera, New Mexico: Results from the Jemez teleseismic tomography experiment. J. Geophys.
679 Res. 103, 24,301 – 24,320.
680
681 Sun, W., and Kennett, B., 2016. Uppermost mantle structure of the Australian continent from Pn
682 traveltime tomography, submitted to Journal of Geophysical Research: solid earth 121(3), 2004-
683 2019.
684
685 VandenBerg, A. H. M., 1999. Timing of orogenic events in the Lachlan Orogen. Aust. J. Earth Sci.
686 46, 691–701.

687 Wallner, H., and Schmeling, H., 2010. Rift induced delamination of mantle lithosphere and crustal
688 uplift: a new mechanism for explaining Rwenzori Mountains' extreme elevation? International
689 Journal of Earth Sceinces 99, 1511–1524.
690
691 Wei, Z., Kennett, B. L. N., Sun, W., 2018. Sn-wave velocity structure of the uppermost mantle
692 beneath the Australian continent, Geophys. J. Int. 213, 2071–2084.
693
694 White, L., Gibson, G., Lister, G., 2013. A reassessment of paleogeographic reconstructions of
695 eastern Gondwana: bringing geology back into the equation. Gondwana Research 24, 984–998.
696 http://dx.doi.org/10.1016/j.gr.2013.06.00
697
698 Yao, H., van der Hilst, R. D., de Hoop, M. V., 2006. Surface-wave array tomography in SE Tibet
699 from ambient seismic noise and two-station analysis - I. Phase velocity maps. Geophys. J. Int.
700 166, 732–744.

701 Young, M. K., Rawlinson, N., Arroucau, P., Reading, A.M., Tkalčic', H., 2011. High-frequency
702 ambient noise tomography of southeast Australia: new constraints on Tasmania's tectonic past.
703 Geophys. Res. Lett. 38, L13313. http://dx.doi.org/10.1029/2011GL047971.

704 Young, M. K., Rawlinson, N., Bodin, T., 2013a. Transdimensional inversion of ambient seismic
705 noise for 3D shear velocity structure of the Tasmanian crust. Geophysics 78. http://dx.
706 doi.org/10.1190/geo2012–0356.1.

707 Young, M. K., Cayley, R. A., McLean, M. A., Rawlinson, N., Arroucau, P., Salmon, M., 2013b.
708 Crustal structure of the east Gondwana margin in southeast Australia revealed by
709 transdimensional ambient seismic noise tomography. Geophys. Res. Lett. 40, 4266–427.

714

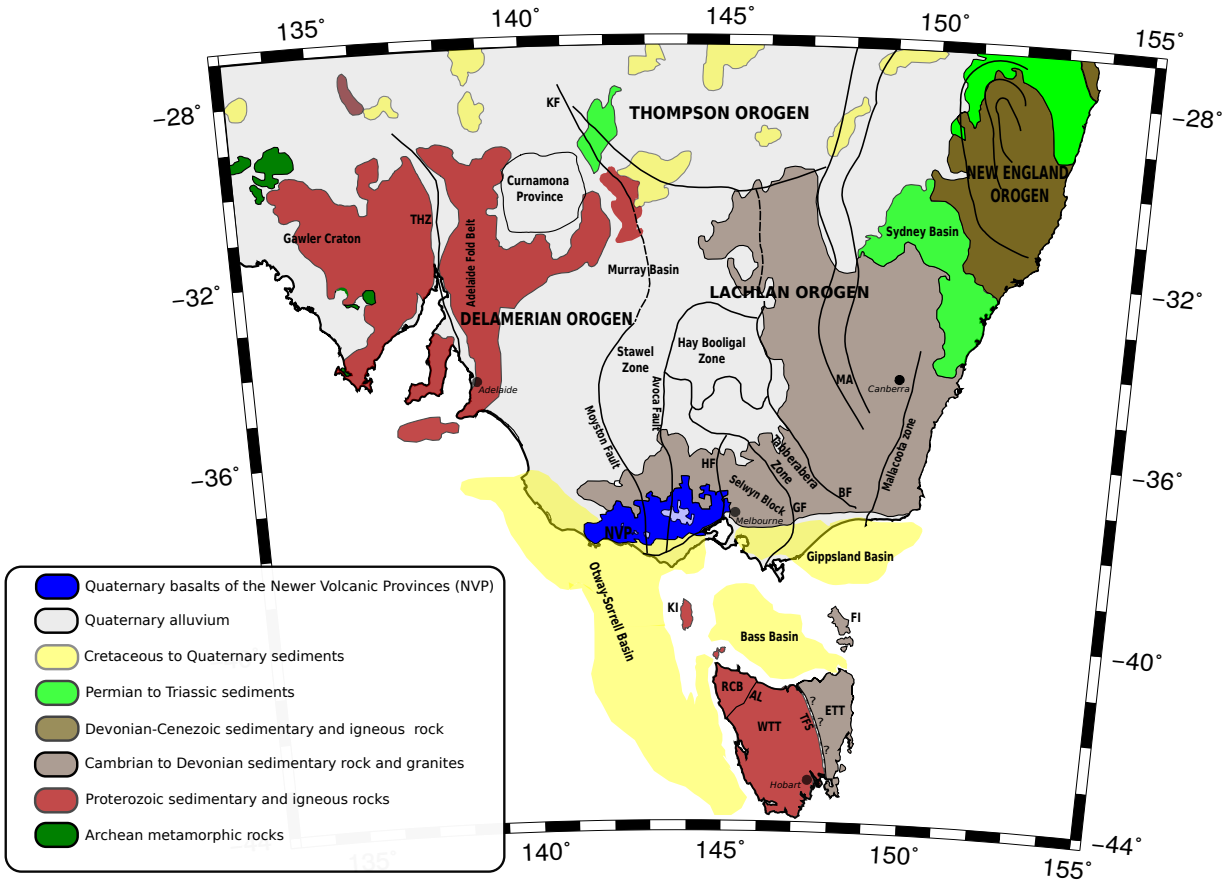

Fig. 1: Simplified geological map of southeastern Australia showing observed and inferred geological boundaries and main tectonic features mentioned in the text. Thick black lines show locations of structural boundaries. KF = Koonenberry Fault; HF = Heathcote Fault; GF = Governor Fault; BF = Bootheragandra Fault; THZ = Torrens Hinge Zone; NVP = Newer Volcanic Province; MA = Macquarie Arc; KI = King Island and FI = Flinders Island in Bass Strait; WTT = Western Tasmania Terrane; ETT = Eastern Tasmania Terrane; AL = Arthur Lineament; TFS = Tamar Fracture System and RCB = Rocky Cape Block.

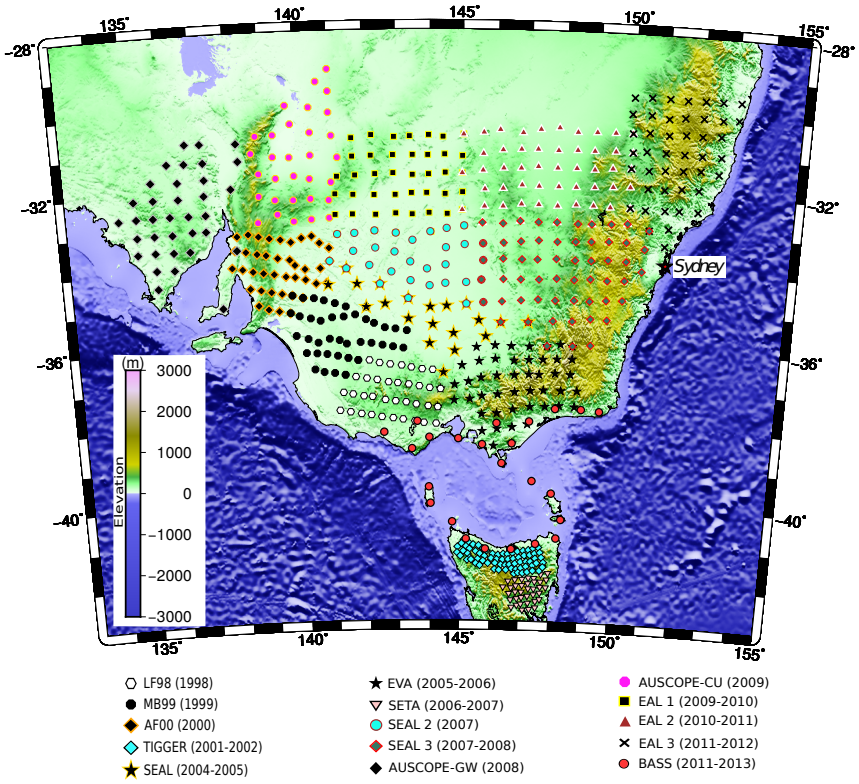

Fig. 2: Topographic/bathymetric map of the study area showing locations of the fifteen different arrays represented by different symbols.

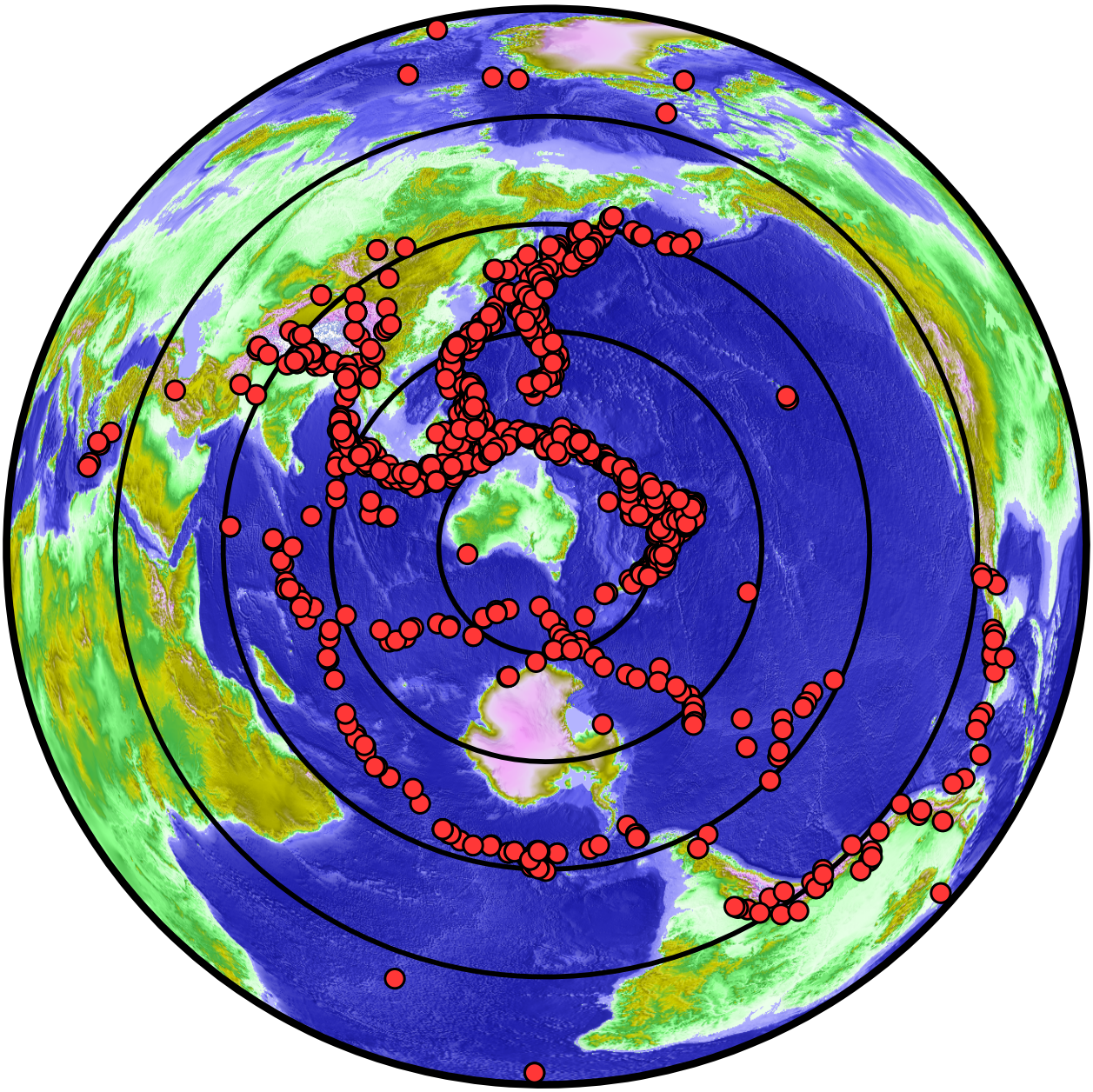

Fig. 3: Distribution of teleseismic events used to constrain the 3-D P wave velocity model. Concentric circles are plotted at 30° intervals from the centre of Bass Strait.

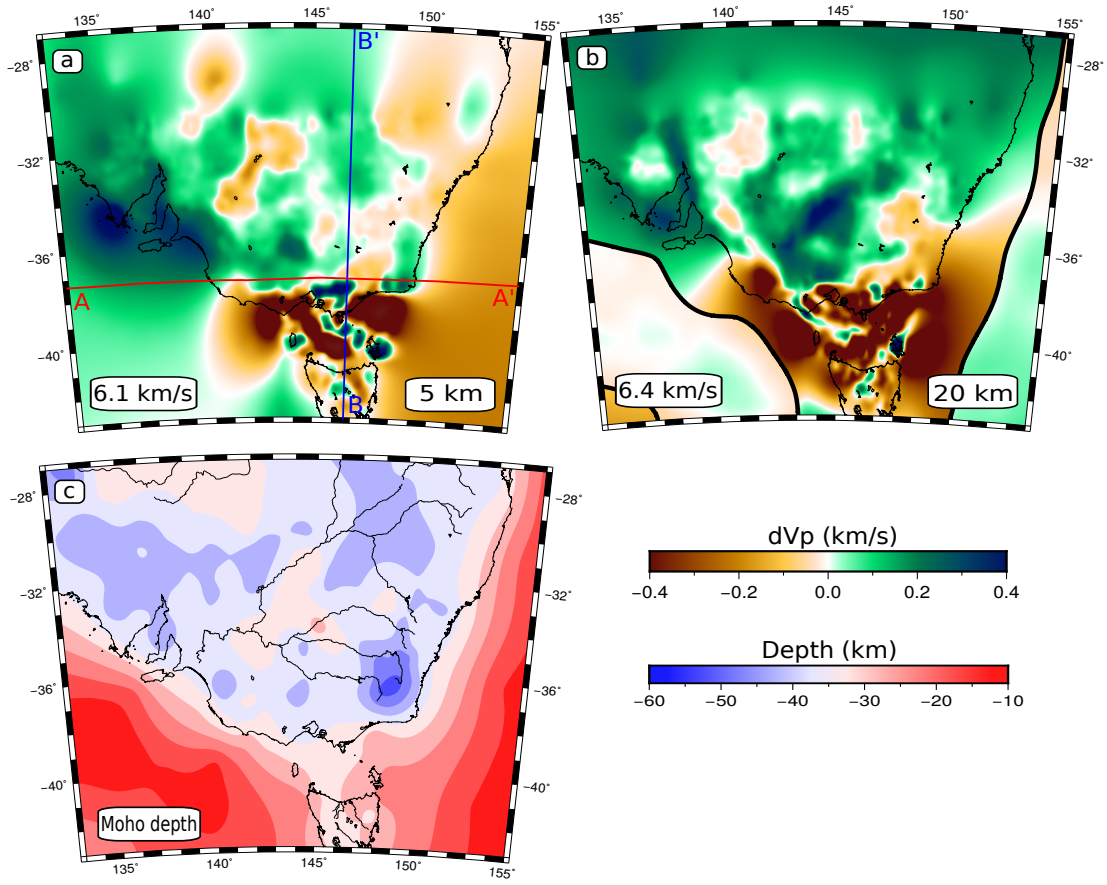

Fig. 4: (a,b) Two depth slices through the new ambient noise crustal model at 5 km and 20 km depth. Since it is the relative velocity variations that are important for teleseismic tomography, perturbations from a laterally averaged depth-dependent 1-D version of the model (see bottom left corner of a,b for reference velocity values) are shown. Thick black lines (see 20 km depth slice in (b)) denote the intersection of the depth slice with the Moho. (c) AuSREM Moho depth model for southeast Australia, which is also used in the starting model of the teleseismic tomography. We have converted the original S-wave velocity model to P-wave velocity, which is what is shown here.

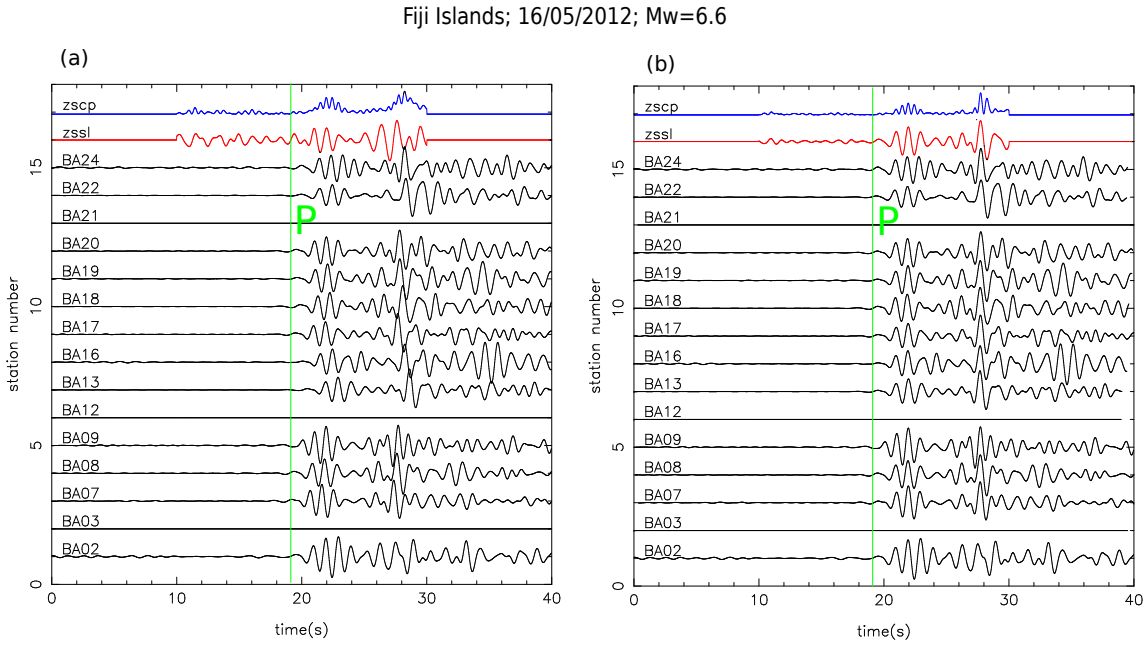

Fig. 5: Example of adaptive stacking of recorded P waves at BASS stations. (a) are the filtered traces before stacking; (b) the filtered traces after stacking. The top blue and red coloured traces are the quadratic stack (zscp) and linear stack (zssl) respectively. The vertical green lines indicate predictions from the global reference model ak135, to which all traces have been aligned in (a).

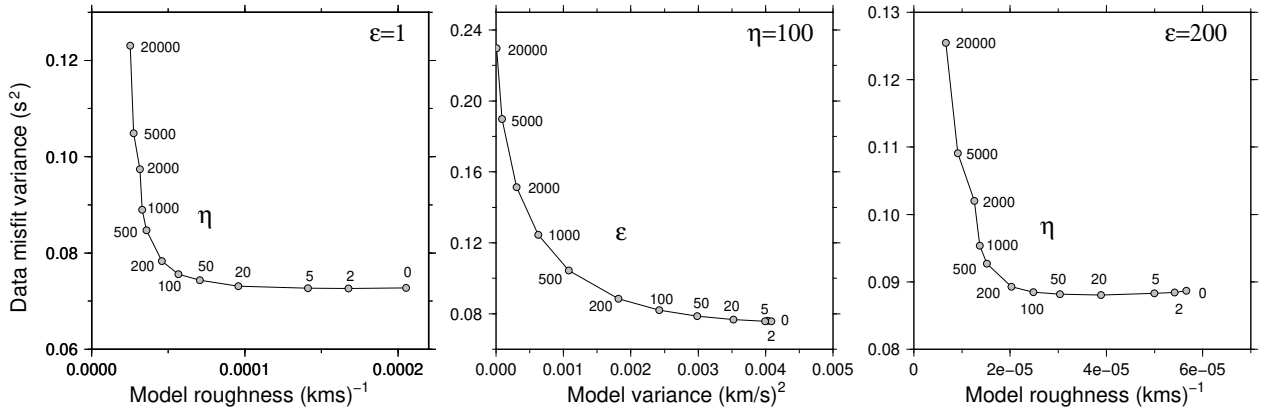

Fig. 6: Trade-off curves used to find optimum damping and smoothing parameters. (a) Vary smoothing parameter while holding damping parameter fixed at $\varepsilon = 1$. (b) Vary damping parameter while holding smoothing parameter fixed at $\eta = 100$. (c) Vary η while holding the damping parameter fixed at the new value of $\varepsilon = 200$. In all the three cases, $\varepsilon = \eta = 200$ appears to be an acceptable choice.

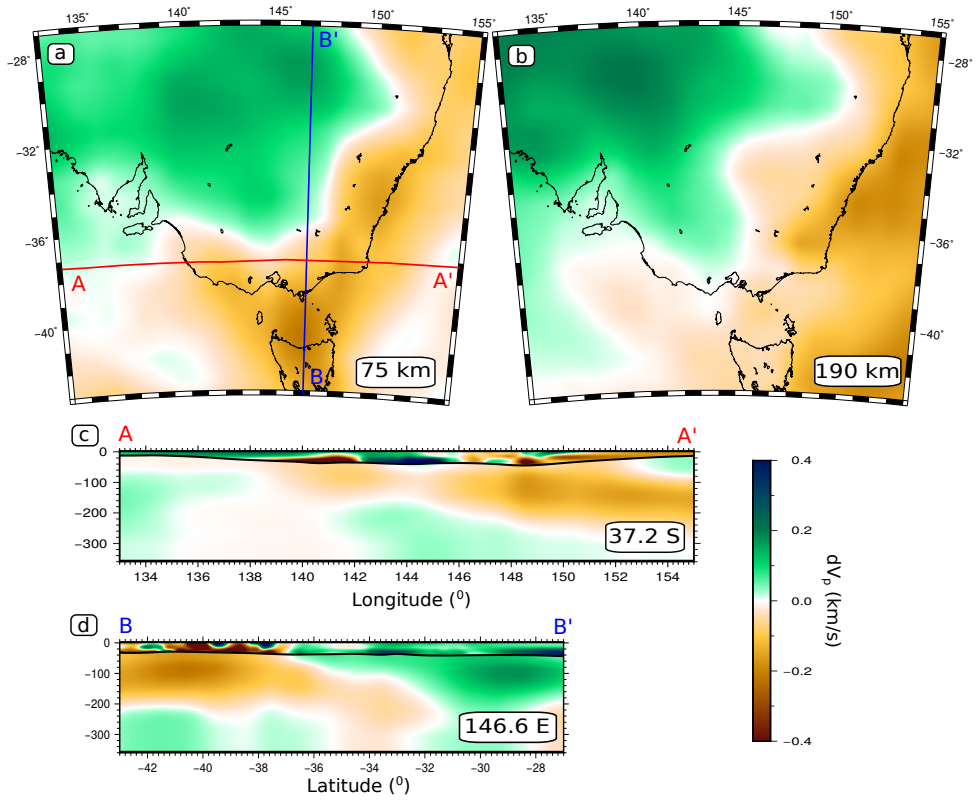

Fig. 7: A selection of slices through the starting model used for teleseismic tomography. (a) 75 km depth slice; (b) 190 km depth slice; (c) EW cross-section at 37.2°S; (d) NS cross-section at 146.6°E. In all cases, velocities are plotted relative to a reference one-dimensional model. The horizontal red line and vertical blue line in (a) denote the cross-section locations of (c) and (d) respectively.

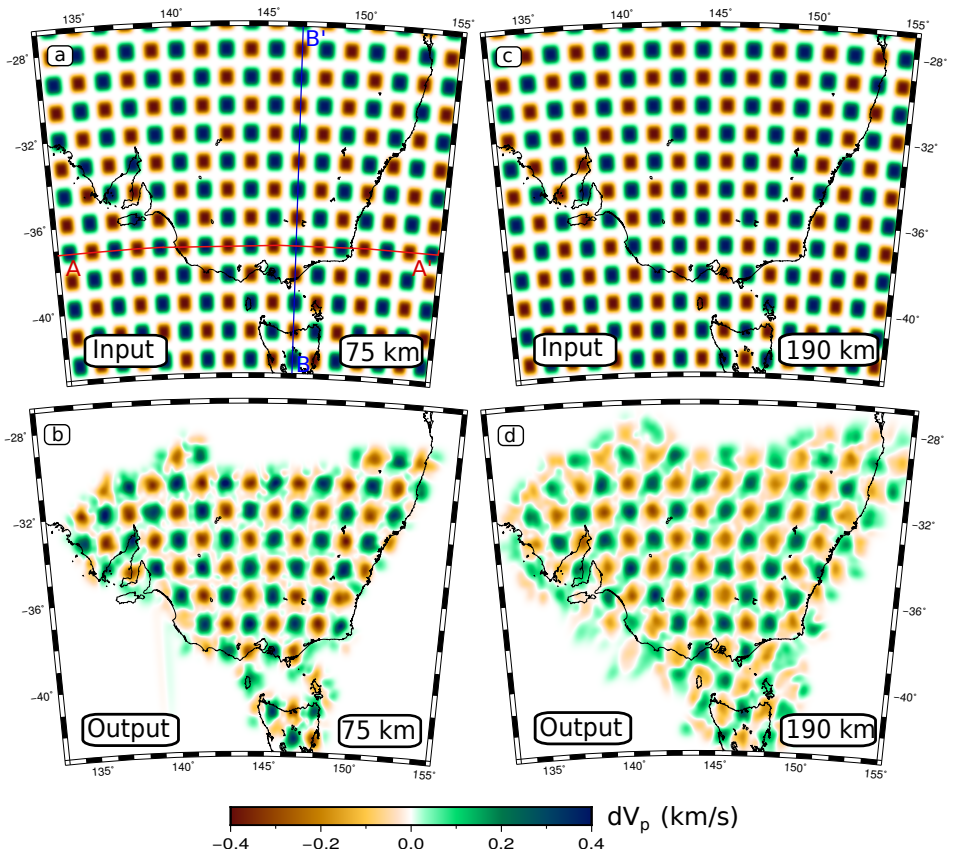

Fig. 8: Depth sections illustrating the synthetic resolution test results. (a) Input test model at 75 km depth; (b) recovered model at 75 km depth; (c) input test model at 190 km depth; (d) recovered model at 190 km depth. The horizontal red and vertical blue lines in (a) denote the cross-section locations of Fig. 9a and b respectively.

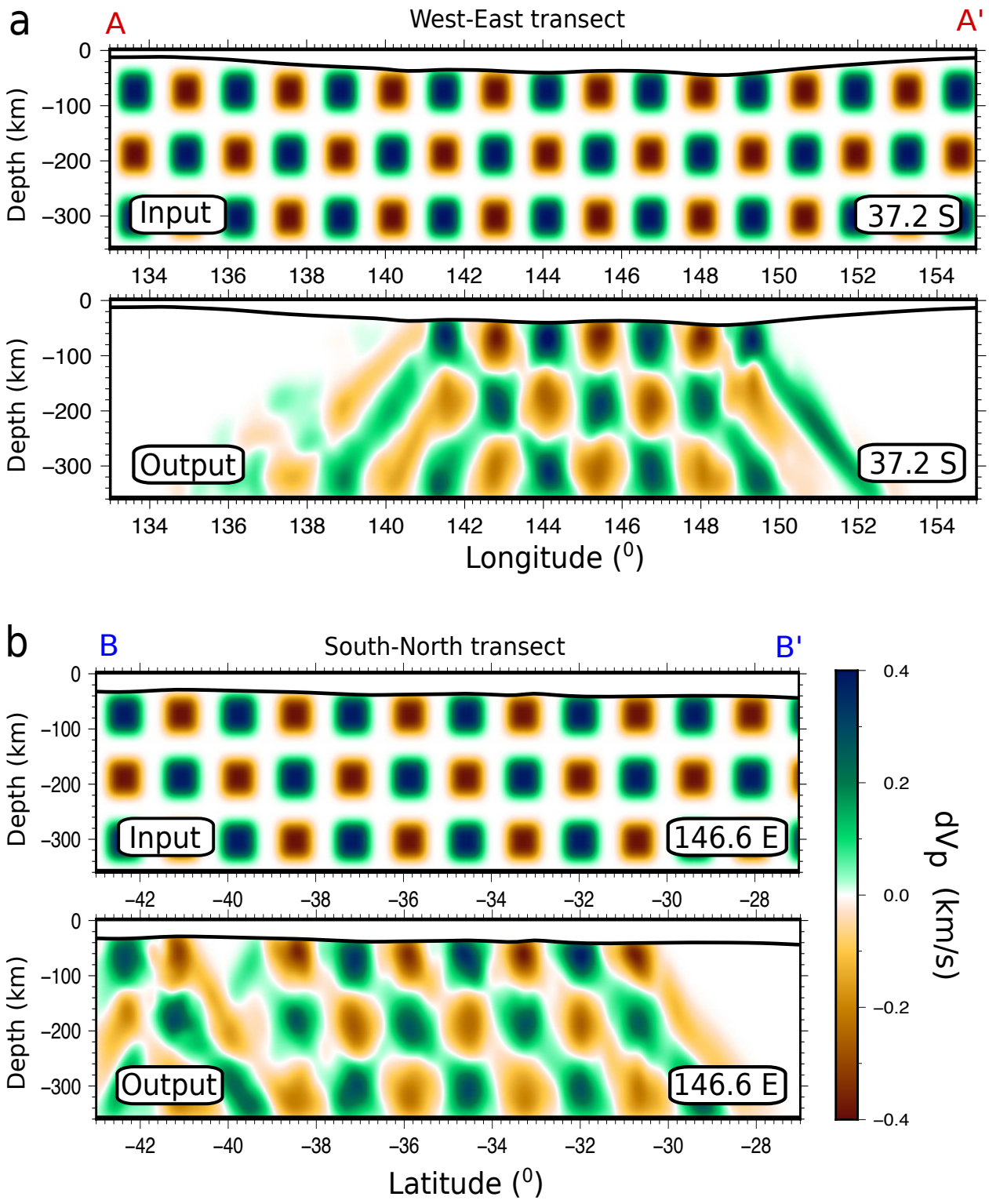

Fig. 9: Cross-sections illustrating the synthetic resolution test results. (A-A') Input and output test models at 37.2°S (see red line in Fig. 8a for location); (B-B') input and output test models at 146.6°E (see blue line in Fig. 8a for location).

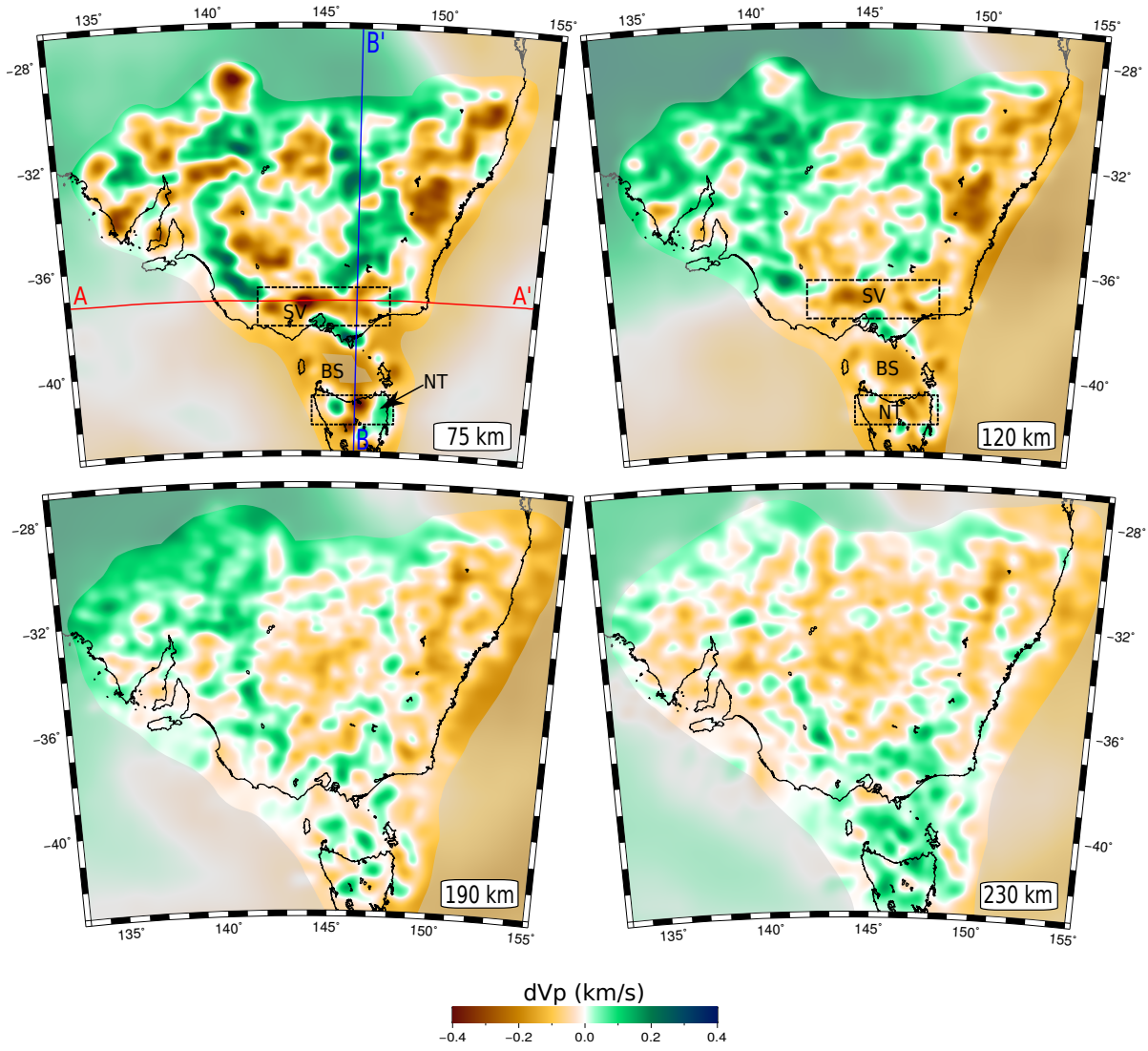

Fig. 10: Horizontal slices through the solution model obtained by inversion of relative arrival time residual data from the WOMBAT and BASS arrays. P-wave speed perturbations are relative to a 1-D depth-averaged version of the model. The gray mask denotes less resolved areas as determined by inspection of checkerboard test results for each depth slice. Several features are highlighted which are discussed in detail in the text: SV = Southern Victoria; NT = Northern Tasmania; BS = Bass Strait.

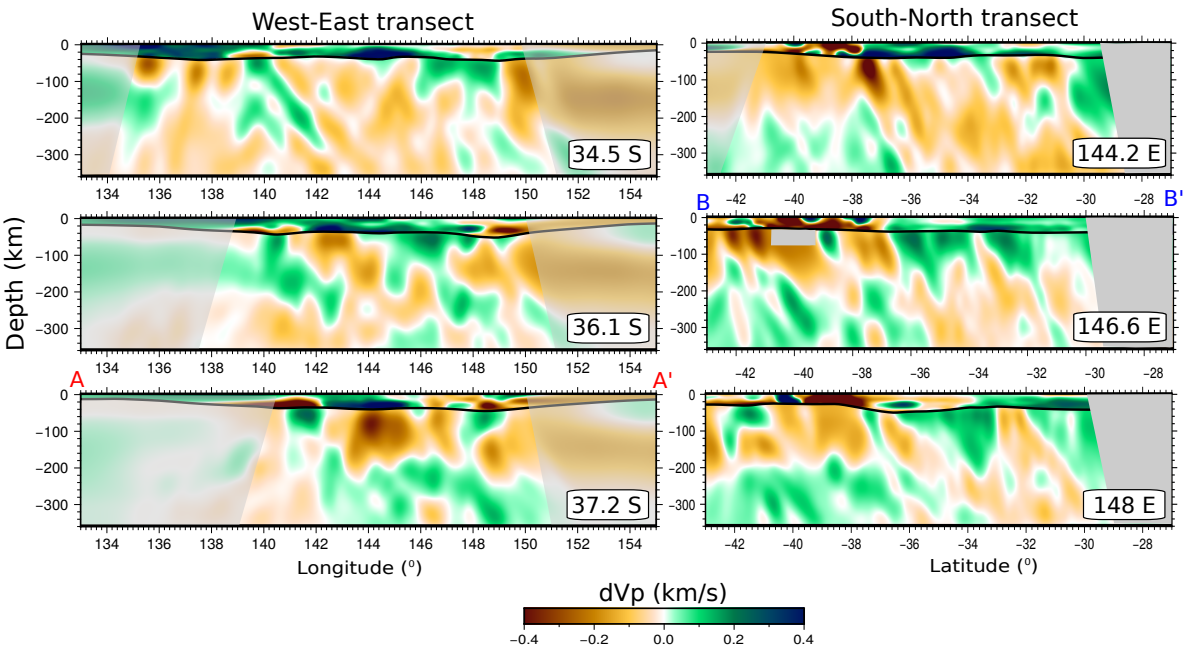

Fig. 11: Vertical slices through the solution model obtained by inversion of relative arrival time residual data from the WOMBAT and BASS arrays. As in Fig. 10, P-wave speed perturbations are relative to a 1-D depth-averaged version of the model. The gray mask denotes less resolved areas as determined by inspection of checkerboard results for each profile. See blue and red lines in Fig. 10 for locations of AA' and BB'.

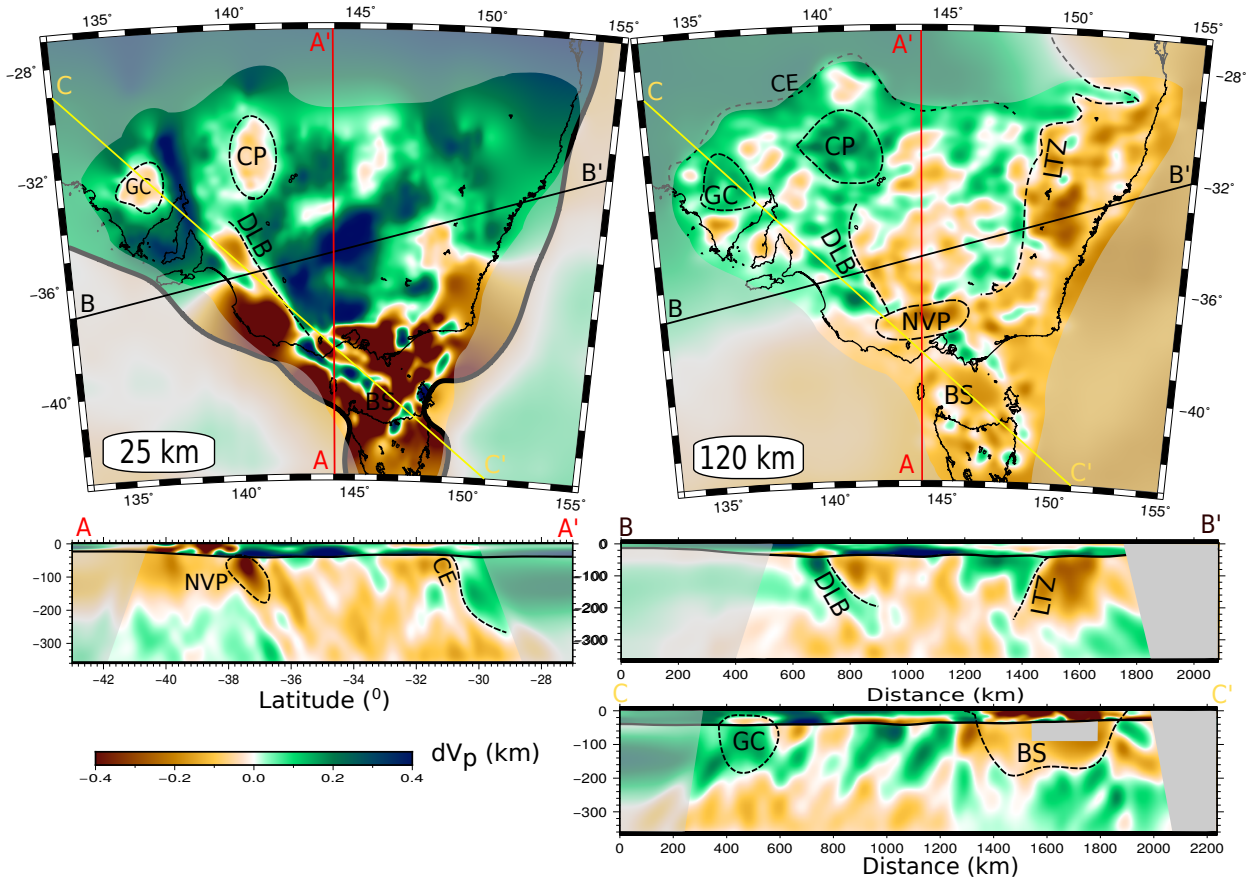

Fig. 12: Slices through the 3-D crust and upper mantle model of southeast Australia which uses the ambient noise crustal model and AuSREM Moho and upper mantle model in the starting model for the teleseismic data inversion. The locations of the three cross sections are denoted in both depth sections as coloured lines. Velocities are plotted relative to a reference one-dimensional model. The gray mask denotes less resolved areas as determined by inspection of checkerboard test recovery for each profile and depth slice. Several features are highlighted which are discussed in detail in the text: DLB = Delamerian-Lachlan boundary; LTZ = Lithosphere Transition Zone; NVP = Newer Volcanics Province; BS = Bass Strait; CE = Craton Edge; CP = Curnamona Province; GC = Gawler Craton. The velocity anomalies identified by the dashed lines are inferred to represent a signature at depth of what is observed at the surface.

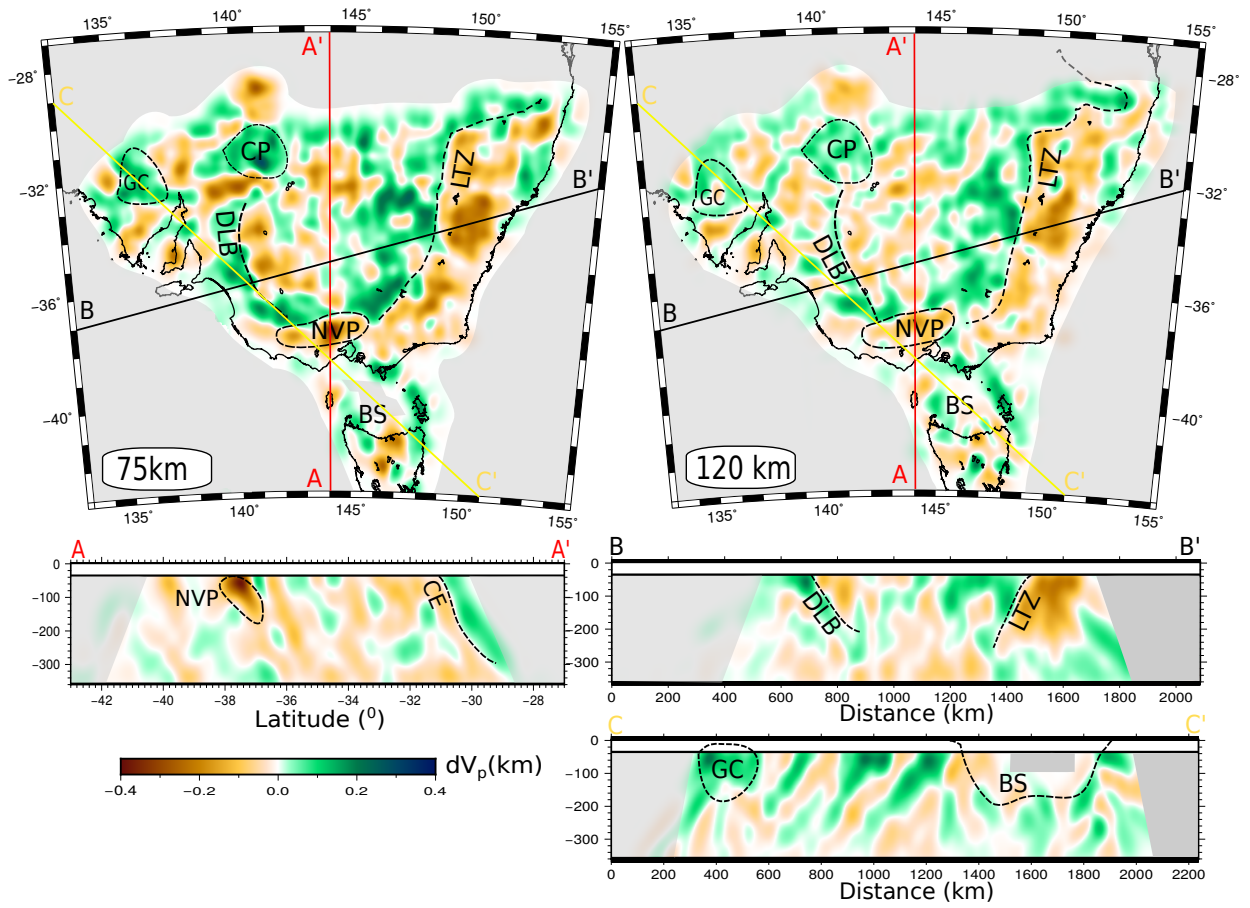

Fig. 13: Same as Figure 12 but now using a 1-D starting model (ak135) and a flat Moho for the teleseismic data inversion. The locations of the three cross sections are denoted in both depth sections as coloured lines. The gray mask denotes less resolved areas as determined by inspection of checkerboard test recovery for each profile and depth slice. Note the poor resolution in upper parts of the Bass Strait. Several features are highlighted which are discussed in detail in the text: DLB = Delamerian-Lachlan boundary; LTZ = Lithosphere Transition Zone; NVP = Newer Volcanics Province; BS = Bass Strait. CE = Craton Edge; CP = Curnamona Province; GC = Gawler Craton. The velocity anomalies identified by the dashed lines are inferred to represent a signature at depth of what is observed at the surface.